Revision 1

Full analysis of feldspar texture and crystal structure by combining X-Ray and Electron techniques

Tonči Balić-Žunić[1], Sandra Piazolo[2,3], Anna Katerinopoulou[1] and Johan Haagen Schmith[4]

[1]Natural History Museum, University of Copenhagen, Øster Voldgade 5-7, DK-1350 Copenhagen K, Denmark

[2]Department of Geology and Geochemistry, Stockholm University, Svante Arrhenius väg, Stockholm, Sweden

[3] Australian Research Council Centre of Excellence for Core to Crust Fluid Systems/GEMOC, Department of Earth and Planetary Sciences, Macquarie University, NSW, 2109, Australia

[4]Department of Geography and Geology, University of Copenhagen, Øster Voldgade 10, DK-1350 Copenhagen K, Denmark

corresponding author: Tonči Balić-Žunić,

Always consult and cite the final, published document. See http://www.minsocam.org or GeoscienceWorld

ABSTRACT

Feldspar crystals typically show a range of exsolution and polysynthetic twinning textures which can present problems for their full characterization, but at the same time give important information about their genesis. We present an integrated procedure for the micro-texture analysis, twin law identification plus crystal structure refinement of all components in a feldspar intergrowth. This procedure was applied to perthitic intergrowths in feldspars from two different pegmatites in the Larvik plutonic complex in the southern part of the Oslo region, Norway. It revealed that the two starting HT feldspars had similar global chemical compositions but underwent significantly different cooling histories, with cooling times probably differing by over an order of magnitude. Powder X-Ray Diffraction with Rietveld refinement was used for a preliminary identification of the mineral components and concluding quantitative phase analysis. Electron Microprobe Analysis was used to bracket the chemical compositions of the constituents. Electron Back-Scatter Diffraction was used to reveal the texture of the samples, twin laws and spatial distribution and crystallographic orientation of the crystal domains. Single-grain X-Ray Diffraction recorded by an area detector was applied for a simultaneous integration of reflection intensities for all crystallographic domains with different orientations and severe diffraction overlaps. The crystal structures were refined using the program JANA2006 which allows a simultaneous calculation for structurally different components. Combined results of various methods helped improving accuracy and resolving ambiguities which may arise from the application of a single technique. The approach is widely applicable to the study of mineral intergrowths and bridges an existing gap in the routinely accessible data on the structural characteristics of rock constituents.

Keywords: feldspar, perthite, X-ray diffraction, Electron back-scatter diffraction, mineral intergrowths, multiphase analysis

Always consult and cite the final, published document. See http://www.minsocam.org or GeoscienceWorld

INTRODUCTION

Feldspars are among the most important minerals in the Earth's crust. They show a broad range of compositional and structural characteristics which present rich information that can be tied to their genesis, but at the same time complicate their analysis. In particular, due to extensive solid solutions at temperatures higher than about 700°C and large immiscibility gaps at lower temperatures, the majority of feldspars begin their history as homogeneous crystals which subsequently exsolve into immiscible components on cooling. The domain structure thus formed is further complicated by frequent twinning inside the homogeneous domains. The two twin laws which are characteristic for this type of transformation twinning are the albite law with the twin axis normal to (010), and the pericline law with the twin axis parallel to [010] direction. In both cases sets of very thin polysynthetic lamellae are formed. These features can present difficulties to the crystal structure analysis by X-ray diffraction and sometimes to other standard analytical methods like optical microscopy and electron microprobe. As a consequence of these difficulties, detailed crystal structure determinations and refinements of various feldspars are not abundant and still do not belong among the routine methods of analyzing feldspars in rocks even though feldspars are of high importance in geology. In this work we attempt to overcome the textural obstacles exploiting the advantages of the area detectors, which have become a standard part of the single-crystal X-ray diffractometers, combined with several other now broadly available analytical techniques. The aim was to achieve a routine integrated approach to a full analysis of the crystal structure, composition and microtexture of feldspars or any other kind of mineral intergrowths.

ORIGIN AND DESCRIPTION OF SAMPLES

The samples analyzed in this study are two perthitic intergrowths of alkali feldspars originating from the Larvik plutonic complex which forms the southernmost part of the Oslo region,

Always consult and cite the final, published document. See http://www.minsocam.org or GeoscienceWorld

Norway. The complex is made up of monzonitic rocks, mainly larvikite and its closely related varieties (Neumann 1980). It consists of 10 semicircular plutons arranged in a manner which suggests a sequential shift of centres of igneous activity towards the west with a progressive higher degree of silica under-saturation (Petersen 1978). The age determinations indicate that the complex was emplaced between 299 and 292 Ma before present (Dahlgren et al. 1996). The igneous rocks are cut by a number of pegmatites, many of them well exposed due to intense quarrying activities around Larvik. Quartz-bearing pegmatites dominate in the east and nepheline-syenite pegmatites in the west (Neumann and Ramberg 1978). The samples investigated in this work are from the latter type pegmatites.

Sample 16 was collected by the first author on the north side of the main road 302 between Stavern and Helgeroa, 400 m west from Jahren Gård and Feriesenter near Gumserød and about 20-30 m east from the macadam road to Gumserød Gaard. The pegmatite, which here is exposed on the ground, houses large grey feldspars, several tens of cm in diameter and full of inclusions of alkaline amphibole, aegirine and ilmenite. Sample 45 was collected by Søren Bernhard Nielsen from a pegmatite embedded in larvikite in Saga quarry and kindly provided for this study. The quarry is situated on the SW side of Strandåsen at Mørje, close to Telemark-Vestfold county border. The feldspars in the pegmatite are represented by dm-sized red crystals.

EXPERIMENTAL PROCEDURES

Figure 1 represents a schematic diagram depicting the combination of various techniques and their integration in form of a flow chart identifying different steps during the iterative refinement procedure. In the following we present the experimental procedures and details for each of the techniques used at the different steps outlined.

Always consult and cite the final, published document. See http://www.minsocam.org or GeoscienceWorld

Powder X-Ray Diffraction (PXRD)

The samples were measured at the X-ray Diffraction Laboratory of the Natural History Museum, University of Copenhagen. Carefully separated, uniformly coloured fragments of the large crystals were grinded in an agate mortar to a fine powder which felt completely smooth under the piston, mounted in sample holders with silicon single-crystal zero-background plates with cavities of 0.5 mm depth and measured on the diffractometer in Bragg-Brentano reflecting configuration. The experimental details of the method applied in this work are presented in Table 1.

The program TOPASv4.0 (Bruker-AXS product) was used for Rietveld analysis (Rietveld 1969) of the data. For the definition of powder-diffraction profiles we used the fundamental-parameters approach (Cheary and Coelho 1992). Due to the preparation of samples and the excellent cleavage of feldspars the allowance for preferred orientaiton was made by refining the March-Dolasse parameters (Dolasse 1986; Table 2). The background was modelled by Chebyshev polynomials up to the 6th order. The emission spectrum of the X-ray tube used in the refinement was refined on the diagram of the standard sample of CeO_2 measured under the same conditions as the investigated samples. The results of the Rietveld refinement are presented in Table 2.

Electron Microprobe Analysis (EMPA)

The samples were measured in the Microprobe Laboratory of the Department of Geography and Geology, University of Copenhagen. Measurements were done on crystal fragments embedded in epoxy, polished and carbon-coated. The experimental details are presented in Table 1. The results of the analysis are presented in Table 3. In each spot the weight percentages of the six oxides were determined compared with the following standards: corundum (for Al_2O_3), hematite (for Fe_2O_3), K-feldspar (for K_2O), albite (for Na_2O) and

Always consult and cite the final, published document. See http://www.minsocam.org or GeoscienceWorld

wollastonite (for SiO_2 and CaO). Corrections of the raw data were performed using the ZAF procedure.

Electron Back-Scatter Diffraction (EBSD) and simultaneous EDS analysis

Crystallographic data were collected using the SEM based EBSD technique (Adams et al. 1993; Prior et al. 1999). Analyses were performed on uncoated thin-sections at the Electron Diffraction Laboratory of the Department of Geology and Geochemistry, Stockholm University. The data were interpreted using Channel 5 analysis suite from HKL Technology (Oxford instruments). Thin-sections were chemically polished using colloidal silica before analyses. The automated data collections were made in a rectangular grid using a beam scan. Further experimental details can be found in Table 1.

During acquisition all individual electron backscatter diffraction patters (EBSPs) were saved and later analysed in different ways. Reflectors identified by image analysis using the Hough transform procedure (Duda and Hart 1972) were compared to the theoretically 70 strongest reflectors according to different so-called match units. Match units are theoretical models that are defined by the crystal lattice and structure parameters. In Step I we used several standard match units based on literature data (Table 4) as would be the procedure without previous information about the nature of the analyzed feldspars. In the third Step of our investigation, we implemented the refined crystal lattice parameters and atomic parameters derived from the X-ray diffraction measurements. Due to the software restrictions where for triclinic case only a primitive Bravais lattice is accepted, it was necessary to transform the data from the standard feldspar orientation (space group C-1) into the P-1 space group accepted by the HKL Channel 5 (see further explanation in the SXRD section). The obtained pole figures have been subsequently interpreted in terms of the standard feldspar orientation and are represented as such in this paper.

Always consult and cite the final, published document. See http://www.minsocam.org or GeoscienceWorld

For both Step I and III we used a so-called "Advanced fit" procedure to improve the automatic indexing of the full crystallographic orientation. We used a setting where the system iterates 3 times to find a progressively better solution. We only allowed data which showed a very good match between the theoretical and calculated reflector positions (MAD – maximum angular deviation of 0.8). The false data i.e., systematic misindexing was removed from the dataset, no other processing was performed.

In order to double-check the correctness of the phase identification using the EBSPs we performed simultaneous chemical analysis using the Oxford Instruments INCA system. Counts for K, Na, Ca and Si α lines were recorded at each analysis point.

In the following, we represent data in several different ways. *Band contrast images* show a combination of surface topography and crystallographic orientation. They are the map of the quality of data dependent on the matching to the theoretically expected values with the best match giving the brightest shade. *EDS maps* give the counts for Na *K*α, respectively K *K*α lines. *Phase distribution maps* are complementary to the previous, with the phase information now obtained from the matching of the Kikuchi bands to either Na- or K-feldspar. *Crystallographic orientation maps* depict different crystallographic orientation in different colours. *Textural component maps* show the difference in misorientation of each point analysis relative to a chosen reference orientation (marked with a cross). The crystallographic information is further presented in pole figures in the (XYZ) reference frame, where Z is out of plane, using equal area, upper- and lower-hemisphere projections.

Single Grain X-ray Diffraction (SXRD)

The measurements were made in the X-ray Diffraction Laboratory of the Natural History Museum, University of Copenhagen. Like for other methods, the experimental details can be found in Table 1. For the sample 16 a nearly equidimensional crystal fragment with

Always consult and cite the final, published document. See http://www.minsocam.org or GeoscienceWorld

approximate dimensions 400x500x600 μm, light grey-green in colour, was selected from among the crushed material. From sample 45 a cylindrical fragment with the height of 100 μm and diameter of 250 μm, light red in colour, was drilled by a diamond-tip drill mounted on the petrographic microscope (microscope attachment made by Olaf Medenbach, Ruhr-University Bochum).

The data collection was performed using the program SMART (Bruker-AXS software) with a routine which covers a full reciprocal sphere (Table 5). An automatic search for Bragg reflections was done by the same program. In both samples the analysis revealed multiple crystals. The individual parameters and orientations of reciprocal lattices in the diffraction picture were revealed through an iterative procedure in the program GEMINI (Bruker-AXS software) from about 1000 reflections with largest I/σ_I harvested from the recorded data. As the program is originally made for the elucidation of a simpler case of two-component non-merohedral twins, it was necessary to rerun it several times to determine all of the components present in the sample. After the two first were determined, their reflections were removed from the list and the search continued on the rest. Ultimately, the completeness was checked by optical inspection of a number of recorded detector frames. The overlay feature of the program SMART was used, where the expected positions of reflections defined from the orientation matrix are marked on the recorded detector frames.

The procedure was greatly helped by the previous knowledge of the unit cell parameters of the constituent components (PXRD) and the supposed twinning law and the mutual orientation of the various components (EBSD). It must be noted that the search program finds always a primitive unit cell. It is obviously important both for the EBSD search routine (see above in the EBSD section) and for the SXRD reciprocal lattice search to work with the primitive setting of the feldspar crystal lattice and not with the usual C (or I) setting.

Always consult and cite the final, published document. See http://www.minsocam.org or GeoscienceWorld

Therefore, we report in Table 5 also the crystal lattice parameters for the P lattice setting. The transformation of the C unit cell of feldspars to the P one is according to the matrix:

1/2 -1/2 0

1/2 1/2 0

0 0 1

and the opposite one (from P to C) is:

1 1 0

-1 1 0

0 0 1

For a satisfactory refinement of the crystal structure, it is essential to obtain the Bragg-reflection intensities through a combined integration where all of the different orientational components in the intergrowth are treated simultaneously with a registration of reflection overlaps. This is possible in the program SAINT+ (Bruker-AXS product) by specifying multiple orientation matrices in the orientation file. After the integration, the unit cell parameters of all the components were refined from the non-overlapped reflections with $I/\sigma_I >$ 10 and the relation matrices between the components were calculated using the same program (deposited material).

The raw reflection file produced through integration and data reduction procedure in the SAINT+ program was treated subsequently by the TWINABS subroutine of the same program in order to make an empirical absorption correction and produce the reflection file in the HKL5 format. Thereafter, the reflection files were read in the program JANA2006 (Petříček et al. 2006) and a multiple phase refinement was done starting from the structure data for K-feldspar taken from Blasi et al. (1987) and those for the albite from Armbruster et al. (1990). Atomic coordinates and anisotropic displacement parameters for all atoms were

Always consult and cite the final, published document. See http://www.minsocam.org or GeoscienceWorld

refined together with the amounts of K and Na at the A site constrained to a full occupancy. The resulting atomic parameters are presented as crystallographic cif-files in Online Resources 1 to 4.

Taking in account the large number of overlaps (Table 5), a combined simultaneous refinement of crystal structures of all components in the intergrowth is preferable, rather than using only the non-overlapped reflections and refining each of the components alone. An exclusion of overlapped reflections would leave out a substantial number from the list, and, what is of even greater danger, systematically exclude parts of the reciprocal space.

For the purpose of the combined refinement, it is most convenient to use a combined file with reflections of all components with appropriately marked overlaps. For this purpose the reflection file with HKL5 format as used in SHELX programs (Sheldrick 2008) is very convenient. On the other hand, the SHELXL program itself can not be used for a simultaneous refinement of data from different crystal structures (it only can treat twin intergrowths) but the program JANA2006 is suited for the multiple-phase refinements and accepts the HKL5 format. The program accepts specification of multiple "twin" matrices and attribution of each of them to a chosen phase for which separate and specific structure parameters can be entered.

RESULTS

Step I: PXRD, EMPA and EBSD

Always consult and cite the final, published document. See http://www.minsocam.org or GeoscienceWorld

In both of the investigated samples PXRD suggested a mixture of K- and Na-feldspar. In the case of K-feldspar components, the refinement of the crystal lattice parameters suggested in the sample 16 a presence of the high-temperature form (a seemingly monoclinic lattice) and in the sample 45 the presence of the low-temperature microcline form. For the Na-feldspar component, a practically pure low temperature albite resulted from the analysis of the lattice parameters in both samples. For the preliminary Rietveld analysis of the patterns we used the crystal structure data of Blasi et al. (1987) for the K-feldspar components and the data of Armbruster et al. (1990) for the Na-feldspar component. We refined only the unit cell parameters, scale factors, crystallite sizes and the preferred orientation as the structure-specific parameters. An attempt in refining the atomic coordinates resulted in unreasonable values of interatomic distances as could be expected for a mixture of different feldspars with many atomic parameters. The results of the constrained refinements are presented in Table 2.

The back-scattered electron images obtained by EMPA instrument gave an indication of the sizes of the single-phase exsolution domains. As can be seen from Figure 2, the diameters of the chemically homogeneous lamellae on the polished surface were <10 μm in thickness in sample 16, whereas they had a much larger thickness, reaching locally to 100 μm, in sample 45. Due to the relatively small beam size of about 5 μm it was possible to obtain relatively reliable chemical analyses of all components in the samples in both cases, although for sample 16 with more difficulty (Table 3). The chemical analysis gave the following average compositions of Na- and K-feldspar components in the two samples: $K_{0.01(1)}Na_{1.01(1)}Ca_{0.01(0)}Al_{1.00(1)}Si_{2.98(1)}O_8$ and $K_{0.86(5)}Na_{0.17(5)}Al_{1.00(2)}Si_{2.99(2)}O_8$ (sample 16) and $K_{0.01(0)}Na_{1.02(2)}Fe_{0.01(0)}Al_{0.99(1)}Si_{2.99(1)}O_8$ and $K_{1.00(1)}Na_{0.04(1)}Al_{0.99(1)}Si_{3.00(1)}O_8$ (sample 45). They are in a very good agreement with the compositions obtained later from the crystal structure refinement (see Step II).

Always consult and cite the final, published document. See http://www.minsocam.org or GeoscienceWorld

For the quantitative orientation data we allowed only very good match between theoretical and measured reflectors in EBSD. The initial indexing rate for Step I was 42.5 % and 44.6% for samples 16 and 45, respectively. It should be noted that surface quality related problems in parts of the analysed areas precluded indexing in ca. 20% and 5% of the total area of samples 16 and 45, respectively (c.f., Figs. 3 and 4). The used theoretical match units are given in Table 4. Band contrast, phase distribution and crystallographic orientation obtained by EBSD combined with simultaneous EDS analysis (Figs. 3 and 4) provided a good idea of what types of feldspars and twin laws could be expected in the two samples and are in accordance with the results of PXRD and EMPA.

For the albite component in the sample 16 the pole figures showed some highly deviating individual measurements interpreted as false data. However, the majority of determinations group in relatively clear unique orientation of the c axis and the two alternative orientations of both a and the b axes (Fig. 5). For the a axis the two directions are observed conforming to the Carlsbad twin law, one of them dominant and the other clearly underrepresented. However, this feature turned out to be a false one during the Step II analysis (see discussion). For the b-axis direction a splitting characteristic for the albite twin can be seen in the pole figure. This feature could clearly not be an artefact and was confirming the presence of this twin law. For the K-feldspar, apart from the false orientations, the majority of the orientations conform to the orientations of the albite components, however without the splitting of the b-axis (Fig. 5). The latter is not to be expected to be observable, anyhow, with the crystal lattice being very close to the monoclinic one. The lamellar structure as indicated by element mapping as well as the phase distribution in this sample has the lineation approximately parallel to the crystallographic (010) plane which is also the composition plane of the albite twin law.

Always consult and cite the final, published document. See http://www.minsocam.org or GeoscienceWorld

For sample 45 both the orientation of the phase lamellae is visible from the phase distribution and chemistry and their traces are parallel to the (100) plane in this case (Fig. 4). From the band contrast the albite twin lamellae in the albite component are also visible. A misorientation suggesting a Carlsbad twin can be registered here as well but also a continuous spread in orientations of the correctly indexed components (both K-feldspar and albite) (Fig. 6). For albite the presence of the albite twinning was obvious both in the pole figures and crystallographic orientation maps, but for K-feldspar no definite conclusion was possible in this stage.

The EBSD results in this Step confirmed thus the presence of the two feldspar phases in both samples and their K-feldspar and Na-feldspar nature and documented the presence of the albite twin lamellae in the albite components plus questionable Carlsbad twins for all components. Very fine lamellar structure of sample 16 documented that no single-phase grain can be separated from this sample, whereas for the sample 45 single phase grains would be in any case under 100 μm in diameter. All this information was of a great help in the succeeding SXRD analysis (see below).

Step II: SXRD

Three components with different orientations were found by SXRD in the sample 16: one representing K-feldspar and two an albite twin of Na-feldspar. In the case of the sample 45 there were in all four components, because both K-feldspar and Na-feldspar exhibited albite twins. No indication of the simultaneous pericline twinning, as usual in many microclines, could be observed. The microscopic inspection of the thin section of the sample 45 also indicated just two twin orientations in both Na- and K-feldspar (Figure 7). Many of the observed reflections were partly or fully overlapping between the components (Table 5). This is a consequence of the albite twin law plus the near correspondence in orientations

Always consult and cite the final, published document. See http://www.minsocam.org or GeoscienceWorld

between the K-feldspar and Na-feldspar components. The orientational relations can be explained by an exsolution from a common single crystal. For example, in the sample 16 the unique K-feldspar component is symmetrically placed between the orientations of the two Na-feldspar albite twins, as observed already from the EBSD results (Fig. 5). The relational matrices between the components and the reflection list with the overlap indications can be found in Online Resources 5 and 6.

The lattice parameters and the values of the bond distances and coordination volumes for tetrahedral coordinations show that the Na-rich component in both samples corresponds to the low albite with Al completely ordered at the T_1o site (Table 6). There are, though, substantial differences in the ordering grade of the K-rich components between the two samples (Table 7). The one from the sample 45 is very close to the known maximally ordered microcline (Blasi et al. 1987). The ordering grade of the K-feldspar from the sample 16 characterizes it as "orthoclase". We use this term in a rather broad sense here, referring to K-feldspars with partial ordering. More important is that the crystal structure data enable us to quantify accurately the ordering of Al and Si over the tetrahedral sites. The obtained results place K-feldspar from sample 16 on the ordering diagram quite close to the intermediate position with almost all Al preferentially ordered in the both of the T_1 sites (Fig. 8). It is further confirmed by the fact that the crystal structure parameters correspond closely to the sample A1D from a systematic work on K-feldspars with a high range of ordering grades from the Adamello Massif (Dal Negro et al. 1978; see Table 7). The amount of Al in the T_1o site is around 50%, but, in accordance with the observations of Dal Negro et al. (1978), it has still not reached this value in T_1m site and the structural symmetry is already a triclinic one. This confirms the slight deviation of the crystal lattice from ideal monoclinic angles as suggested by the refinement of crystal lattice parameters which can thus be considered significant. In other words, the K-component has in the ordering process already passed the

Always consult and cite the final, published document. See http://www.minsocam.org or GeoscienceWorld

field of sanidine and entered the intermediate-microcline state. Likewise, our data confirm the previously observed deviation from an ideal two-step ordering path in K-feldspar (Fig. 8).

The compositions of the two K-feldspars obtained through crystal structure refinement are $K_{0.86(1)}Na_{0.14(1)}AlSi_3O_8$ and $K_{0.93(1)}Na_{0.07(1)}AlSi_3O_8$ for the samples 16 and 45, respectively, which corresponds very good with the EMPA results.

Step III. Refined EBSD, final Rietveld refinement of PXRD data.

With the knowledge of the crystal lattice and crystal structure parameters from SXRD, we performed the orientation analysis using the same EBSPs acquired for the two samples in Step I. The indexing percentage changed markedly (see Table 4) and the data were much more reliable, e.g., points that were indexed as K-feldspar were consistently in areas of high K content (Figs. 3 and 4). Although the introduction of the crystal structure data from SXRD improved the indexing and especially for the sample 45 removed several inaccuracies from the pole figures, some reflectors still remained with an alternate direction of the a axis as mentioned under Step I, corresponding to what can be regarded as the Carlsbad twinning where the two crystal lattices are related by a 180° rotation around the c axis. This is contrary to the SXRD results where no twinning of this kind could be observed. EBSD results can be explained as common misindexing in feldspars. Both the period of the [-1 0 -1] direction and its angle to the *c* axis correspond closely to those of the [100] direction. The difference in the periods and angles is only about 2% in the K-feldspar and lower than 1% in albite. SXRD is discriminative enough to detect the presence of Carlsbad twins because of its good angular resolution and the fact that it records the diffraction from all parts of the sample simultaneously. In the case of EBSD the orientation is judged from Kikuchi bands of individual reflectors and the mistake is in the range of the accuracy of the method. Our results confirm this potential ambiguity in the analysis of feldspars and show that for the final

Always consult and cite the final, published document. See http://www.minsocam.org or GeoscienceWorld

confirmation of the presence or absence of Carlsbad twinning a SXRD analysis might be needed. In principle, the Carlsbad twinning should be characterized by relatively well defined domains already in EBSD. It is a penetration twin consisting of just two domains and although the contact surface can be complex, the crystallographically defined twins should correspond to spatially well defined areas with distinct boundaries on EBSD orientation contrast images. In the case of sample 16 and 45 such spatial relationships were not identified.

EBSD analysis shows the textural details of the samples (Figs. 3, 4, 6, 9). In sample 16 the lamellae appear to be parallel to the (010) plane. Our results thus suggest conformity of the exsolution lamellae and the twin lamellae of the albite component.

In sample 45 the angular spread of orientations for all components is about 6° (Fig. 9). In spite of the angular spread, the albite twin components in albite are clearly visible also on pole figures (Fig. 6), because the orientations of the angular deviation of the twin splitting and the angular spread are different. Furthermore, the twin components are clearly discernable in the orientation map. For the K-feldspar the situation is not so clear. The angular spread is larger than the expected split angle of 4.7^{o} for an albite twin in microcline. Unfortunately, the orientation of the angular spread also coincides with the direction of twin splitting masking it on the pole figures of relatively large areas as the one represented on Figure 6. In this way, although the albite twinning in microcline observed by SXRD can not be excluded, it can also not be completely confirmed by EBSD if bulk data are considered. However, by selecting data from smaller homogeneous areas, a clear splitting of the b axis in the two directions conforming to the albite twin law became visible (black boxes, Fig. 6). SXRD results suggest that one of the twin domains in microcline is much more dominant than the other; in other words one of the two twin components occupies much larger volume than its counterpart. The same relationship is also seen in the EBSD data, where one twin orientation occupies a much smaller area than its twin counterpart (bright blue data points in Fig. 6).

Always consult and cite the final, published document. See http://www.minsocam.org or GeoscienceWorld

Powder diffraction analysis is superior to other analytical methods in the quantitative determination of the proportions of phases in the intergrowth. As well documented (see e.g., Shim et al. 1996; Balic-Zunic et al. 2011) for a reliable quantitative phase analysis the refinement of the preferred orientation is mandatory in the case of crystals with prominent cleavage. In this case we used a combination of the March-Dolasse function (Dolasse 1986) for the two crystallographic planes known to represent the cleavage directions in feldspars. As could be expected, the (0 0 1), being the more prominent cleavage, showed a clearly pronounced effect, whereas the (0 1 0) practically had no effect on preferred orientation (Table 2).

Comparison of the results based on the literature data and those based on the atomic parameters obtained by the SXRD (Table 2) shows small differences for sample 16 and no significant differences for sample 45. As mentioned in Step I, the Rietveld refinement had to be constrained to assumed atomic parameters. Our results show that even with such constrained refinements one can obtain highly accurate unit cell parameters for albite and K-feldspar mixtures. The use of the accurate atomic parameters obtained through SXRD improves the results of the quantitative phase analysis in the case of sample 16 where the ordering grade of K-feldspar does not match the used literature reference data. It is interesting that we obtain relatively good results in Step I in spite of using the crystal structure parameters of the low microcline. To test the influence of various structural parameters, we tried also refinements with the starting parameters corresponding to the sample A1D from Dal Negro et al. (1978) which matches closely our results from SXRD and the sample P2B which represents the most disordered K-feldspar from the same work. The resulting proportions of albite and K-feldspar from these two refinements were 57:43 and 58:42, respectively, to be compared to the “real” values of 56:44 (Table 2).

Always consult and cite the final, published document. See http://www.minsocam.org or GeoscienceWorld

The data of the quantitative phase analysis combined with the results of the chemical analysis (EMPA and SXRD) of the separate phases enable us to calculate the average composition of the starting high-temperature homogeneous feldspar. They are $Or_{0.37}Ab_{0.63}$ and $Or_{0.43}Ab_{0.57}$ for the samples 16 and 45, respectively (neglecting the minor An component in the sample 16).

DISCUSSION AND CONCLUSIONS

Our analyses show that sample 16 represents a mesoperthite (Smith and Brown 1988) with an exsolution texture consisting of lens-like lamellae with the shortest diameter under 10 μm. Albite dominates volumetrically over K-feldspar and contains two sets of lamellae twinned after the albite law. The K-feldspar lamellae have $Or_{86}Ab_{14}$ composition and an almost monoclinic crystal lattice with the orientation intermediate between the two twin components of albite. The orientation maps suggest that the long phase domain boundaries are parallel to the (010) twin plane. The structure of the albite corresponds to low albite and that of the K-feldspar to the partially ordered intermediate microcline (orthoclase). The structural and textural characteristics suggest that the coarsening of the exsolution lamellae has stopped in this sample in its incipient stage and the time or temperature was not enough for a maximum ordering in the K-feldspar phase.

Sample 45 represents again a mesoperthite with an average composition similar to the sample 16, with an exsolution texture consisting of coarse lamellae with mostly straight and sharp boundaries with the short diameter reaching up to about 100 μm. Again, albite is in a small surplus and contains two sets of lamellae twinned after albite law. The lamellae of K-feldspar have $Or_{93}Ab_{07}$ composition and are also twinned according to the albite law. The structure of the albite corresponds to low albite and that of the K-feldspar to the maximally

Always consult and cite the final, published document. See http://www.minsocam.org or GeoscienceWorld

ordered low microcline. The long phase boundaries in this case are parallel to the (100) plane. The pericline twin law could not be confirmed either optically or analytically.

The two antiperthites formed by exsolution from homogeneous alkali feldspars which both had a composition very close to 60 mol% Ab and 40 mol% Or. The cooling history ended differently for the two samples, as well documented by the textural and crystal structure characteristics. For the sample 45 a relatively slow and longer cooling can be assumed, whereas the exsolution texture and degree of ordering of K-feldspar in the sample 16 suggests a significantly shorter cooling history. Using the TTT diagram of Parsons and Brown (1984), we can conclude that the development in the sample 16 resembles roughly their curve E' with an estimated cooling time estimated to about 1000 y, whereas the sample 45 matches better curves F to H with an estimated cooling time of over 10000 y. It should be noted that this result mostly depends on the accuracy of the estimated time necessary for the beginning of monoclinic to triclinic transition and time necessary for the full ordering of Al and Si, respectively, in the K-feldspar, which produces in TTT diagram a difference of at least one order of magnitude in time.

The two samples show not only largely different textures, but also a different spread of crystallographic orientations. In the sample 45 with longer cooling history and higher degree of exsolution development and structural ordering, the deformation spread of orientations is higher, about 6° over the investigated area (Fig. 9), and actually masks the K-feldspar twinning. This feature is most probably related to the strain relaxation in the coarsely textured antiperthite caused by the ordering and change of the crystallographic symmetry in K-feldspar which would be in accordance with its orientation (the deformation spread is parallel to the split in the orientation of the b-axis in the two K-feldspar twin components).

Always consult and cite the final, published document. See http://www.minsocam.org or GeoscienceWorld

As the purpose of this work is the evaluation of the combined experimental procedure, we do not venture in further geological interpretation of results for which a more systematic study on a larger body of samples from Larvik plutonic complex is needed.

We have utilized and combined four different experimental techniques in the analysis of the feldspar intergrowths. Each of them has aspects which can not be satisfactory covered by any of the others if truly quantitative data should be obtained. Combining the methods does not only bring a more complete picture of the sample. Also the individual results are improved through synergetic influence. In the following, we discuss those aspects of the various applied methods in some detail.

Diffraction analysis of the powdered sample (PXRD) reveals the main mineral constituents and gives their accurate crystal lattice parameters. It is therefore a valuable tool in the start of the combined analysis. It can also be performed relatively quickly due to easy preparation of samples and a short acquisition time compared to other methods. Diffraction analysis together with the other preliminary analyses (EMPA, EBSD) form the important background for the understanding of the features of SXRD and the full refinement of the crystal structures of all the individual phases.

The Rietveld refinement is used for the analysis of all aspects of the PXRD data. Unlike different other previously used methods, the Rietveld method does not need individual extraction of diffraction maxima for a refinement of crystal lattice parameters and is in large part self-correcting through coupling of the various parameters and their functions. Feldspars are low-symmetry structures with a large number and a high overlap of diffraction maxima. In the case of a mixture of alkali feldspars, our results show that reliable results for crystal lattice parameters can be obtained if the Rietveld analysis is based on atomic parameters of ordered albite and microcline. Rietveld analysis can therefore be applied already at the beginning, before the accurate atomic parameters are known from SXRD. Our results show that

Always consult and cite the final, published document. See http://www.minsocam.org or GeoscienceWorld

relatively accurate crystal lattice parameters and even quantitative proportions can be obtained by using the crystal structure parameters of a completely ordered microcline even if the real sample is only partially ordered. The obtained lattice parameters did not allow classification of the K-feldspar as low sanidine (monoclinic) or partially ordered microcline (triclinic), due to a very small deviation of α and γ angles from orthogonality. Inability to refine unconstrained atomic parameters and the very small differences obtained with constrained refinements based on K-feldspars with different degrees of order in the case of sample 16, show the weakness of PXRD in characterizing the degree of order in feldspars. This aspect, however, can be treated satisfactory with SXRD.

Whereas fully accurate atomic parameters are not needed for the preliminary values of the crystal lattice parameters which can be used for EBSD and SXRD, they are needed for a fully accurate quantitative phase analysis. It can be seen that the preliminary analysis of the sample 45 gave already accurate mineral proportions, because the crystal structure models used in Rietveld refinement matched closely those of the minerals present (low albite and low microcline). In the case of the sample 16, the results of the quantitative phase analysis can differ by several % if the wrong degree of order is assumed for the K-feldspar. This has to be taken in account if partially ordered feldspars are present in the mixture.

Electron Microprobe Analysis gives important information about the chemical composition of the sample. In the case of very fine exsolution textures the spatial resolution may hamper the determination of the accurate composition of individual components. In this case, the SXRD refinement can give the chemical composition of the exsolved phases, especially when bracketed by the preliminary EMPA results.

EBSD is superior in determining the textural relationships of the sample. Accurate crystal lattice and crystal structure parameters obtained by SXRD can improve the resolution and resolve some ambiguities in the case of feldspars. One of the main drawbacks of the

Always consult and cite the final, published document. See http://www.minsocam.org or GeoscienceWorld

EBSD analysis is that without care, systematic misindexing may be interpreted as the existence of twin laws. Careful assessment of the band contrast, chemical composition variation and degree of match between theoretical and experimental reflector orientations is needed, together with a critical evaluation of the potential twin laws (e.g., their known textural characteristics). The two way integration of EBSD and SXRD provides improved data for both analysis techniques. Furthermore, continuous advancement in the algorithms of automatic EBSD pattern analysis will ensure less misindexing.

SXRD is shown to be capable of getting the accurate crystal structure data even from complex intergrowths with several components differing in orientation, thanks to the modern instrumental advances and novel computational methods. It can provide the crystallographic information about the twin laws and the mutual orientation of the various components and the full structural state (degree of order and its features) of each component. Addressing such a complex case as a feldspar intergrowth is substantially aided by a previous knowledge provided by other three methods applied. It largely helps searching the realistic results among the possible solutions calculated by the programs which seek to resolve the diffraction picture into crystallographic components. This technique can not provide the textural information accessible by EBSD or substitute the quantitative phase analysis of PXRD. The bulk chemical composition of the components can be relatively accurately calculated from the results of the crystal structure refinement, but of course no trace element composition which has to be obtained by EMPA.

It is difficult to judge in this case which set of the unit cell parameters can be regarded more accurate, the one obtained from the PXRD or the one obtained from SXRD. In the case of PXRD the complicating factor is the low symmetry of the both phases in the mixture and the large overlap resulting in broad diffraction maxima, especially in the high-angle region of the pattern. In SXRD the patterns are again severed by partial overlap of diffraction spots,

Always consult and cite the final, published document. See http://www.minsocam.org or GeoscienceWorld

both between the different phases and between the non-merohedral twin components. This can result in inaccuracies of the angle determination for the influenced diffraction spots. The additional severing factors are the use of the shorter wavelength and generally more complex three-dimensional aspect of the experiment which is more difficult to calibrate accurately. However, the results of the both methods show a satisfactory agreement (compare Tables 2 and 5) and no substantial difference in crystal chemical interpretations is introduced by choosing any of them. We choose to use the crystal lattice parameters as obtained from SXRD and their calculated esd.s for the report of geometric structural parameters and the crystal chemical comparisons (Tables 6 and 7).

Our results show that accurate information about the various structural properties of feldspar intergrowths and other similar materials can be obtained by the integration of the here applied methods; from the full details of the crystal structure of each component, to the twin and topotactic relations and finally a complete chemical content of the system. We restricted ourselves to still not widely used methods (apart from EMPA) with potentials of new insights. Therefore no high resolution transmission electron microscopy was attempted on the present samples, although it could resolve one remaining open question of this study – the finer (sub-micron) textural details of the sample 16, where our results suggest unexpectedly that the long phase boundaries are not perpendicular, but probably parallel to (010) plane, contrary to a number of previous high-resolution electron microscopy observations on perthites (Parsons and Brown 1984). The latter analyses are already well established in investigations of feldspar intergrowths, whereas the purpose of this study was to establish analysis of crystal intergrowths on another still largely missing level where no routine approaches have been developed so far. The methods applied here and the approach we developed bridge an important gap on a mesoscopic level between the well established and largely applied nanoscopic high-resolution electron microscopy observations of the finest

Always consult and cite the final, published document. See http://www.minsocam.org or GeoscienceWorld

details of intergrowths and the macroscopic observations in field studies. Our results show that the experimental and computational development has reached the state where the additional properties, from the detailed crystal structure to the details of crystal growth and deformation, can be accurately and routinely analysed also in the most complex cases of crystal intergrowths in feldspars or in any other solid material. We believe that the approach has a very broad application field in geological and materials science investigations.

ACKNOWLEDGEMENT

Søren Bernhard Nielsen was of indispensable help in providing the samples for this study. We also thank Alfons Berger for the help in making EMPA analyses. The work of the Copenhagen team was supported by a grant from the Danish Agency for Science, Technology and Innovation. Australian Research Council Centre of Excellence for Core to Crust Fluid Systems/GEMOC, The Macquarie University New Staff Grant is acknowledged by SP. This is contribution 187 from the ARC Centre of Excellence for Core to Crust Fluid Systems (http://www.ccfs.mq.edu.au) and 830 in the GEMOC Key Centre (http://www.gemoc.mq.edu.au). The Knut and Alice Wallenberg foundation is acknowledge for funding the EBSD facility at the Department of Geological Sciences, Stockholm University.

We thank Piera Benna, the other anonymous referee, and the associate editor Anton Chakhmouradian for their useful suggestions in improving the text of the article.

REFERENCES CITED

Adams, B.L., Wright, S.I., and Kunze, K. (1993) Orientation Imaging - the Emergence of a New Microscopy. Metallurgical Transactions A-Physical Metallurgy and Materials Science, 24, 819-831.

Always consult and cite the final, published document. See http://www.minsocam.org or GeoscienceWorld

Armbruster, T., Buergi, H.B., Kunz, M., Gnos, E., Broennimann, S., and Lienert, C. (1990) Variation of displacement parameters in structure refinements of low albite. American Mineralogist, 75, 135-140.

Balic-Zunic, T., Katerinopoulou, A., and Edsberg, A. (2011) Application of powder X-ray diffraction and the Rietveld method to the analysis of oxidation processes and products in sulphidic mine tailings. Neues Jahrbuch für Mineralogie - Abhandlungen, 188, 1, 31-47.

Blasi, A., de Pol Blasi, C., and Zanazzi, P.F. (1987) A re-examination of the Pellotsalo microcline: Mineralogical implications and genetic considerations. Canadian Mineralogist, 25, 527-537.

Cheary, R.W. and Coelho, A.A. (1992) A fundamental parameters approach to X-ray line-profile fitting. Journal of Applied Crystallography, 25, 109-121.

Dahlgren, S., Corfu, F., and Heaman, L.M. (1996) U–Pb time constraints, and Hf and Pb source characteristics of the Larvik plutonic complex, Oslo Paleorift. Geodynamic and geochemical implications for the rift evolution. V.M. Goldschmidt Conference, Journal of Conference Abstracts, 120, Cambridge Publications.

Dal Negro, A., de Pieri, R., Quareni, S., and Taylor, W.H. (1978) The crystal structures of nine K feldspars from the Adamello Massif (Northern Italy). Acta Crystallographica B, 34, 2699-2707.

Dolasse, W.A. (1986) Correction of intensities for preferred orientation in powder diffractometry: Application of the March model. Journal of Applied Crystallography, 19, 267-272.

Duda, R.O. and Hart, P.E. (1972) Use of the Hough Transformation to Detect Lines and Curves in Pictures. Communications of the ACM, 15, 11–15.

Always consult and cite the final, published document. See http://www.minsocam.org or GeoscienceWorld

Finney, J.J. (1962) The crystal structure of carminite and authigenic maximum microcline. Thesis, University of Wisconsin.

Fleet, S.G., Chandrasekhar, S., and Megaw, H.D. (1966) The structure of bytownite ('body-centred anorthite'). Acta Crystallographica, 21, 782-801.

Neumann, E.R. and Ramberg, I.B., Editors (1978) Petrology and geochemistry of continental rifts: Volume I . D. Reidel Publishing Company, Dordrecht.

Neumann, E.R. (1980) Petrogenesis of the Oslo Region larvikites and associated rocks. Journal of Petrology, 21, 499-531.

Parsons, I. and Brown, W.L. (1984) Feldspars and the thermal history of igneous rocks. In W.L. Brown, Ed, Feldspars and Feldspathoids, p. 317-371. D. Reidel Publishing Company, Dordrecht.

Petersen, J.S. (1978) Structure of the larvikite-lardalite complex, Oslo-Region, Norway, and its evolution. Geologischen Rundschau.

Petricek, V., Dusek, M., and Palatinus, L. (2006) JANA2006. Institute of Physics, Czech Academy of Sciences, Prague, Czech Republic.

Prince, E., Donnay, G., and Martin, R.F. (1973) Neutron diffraction refinement of an ordered orthoclase structure. American Mineralogist, 58, 500-507

Prior, D.J., Boyle, A.P., Brenker, F., Cheadle, M.C., Day, A., Lopez, G., Peruzzo, L., Potts, G.J., Reddy, S., Spiess, R., Timms, N.E., Trimby, P., Wheeler, J., and Zetterström, L. (1999) The application of electron backscatter diffraction and orientation contrast imaging in the SEM to textural problems in rocks. American Mienralogist, 84, 1741-1759.

Rietveld, H.M. (1969) A profile refinement method for nuclear and magnetic structures. Journal of Applied Crystallography 2, 65-71.

Always consult and cite the final, published document. See http://www.minsocam.org or GeoscienceWorld

Sheldrick, G.M. (2008) A short history of SHELX. Acta Crystallographica, A64, 1, 112-122.

Shim, S.H., Kim, S.J., and Ahn, J.H. (1996) Quantitative analysis of alkali feldspar minerals using Rietveld refinement of X-ray diffraction data. American Mineralogist, 81, 1133-1140.

Smith, J.V. and Brown, W.L. (1988) Feldspar minerals, vol. I. Springer-Verlag, Berlin.

Winter, J.K., Ghose, S., and Okamura, F.P. (1977) A high temperature study of the thermal expansion and the anisotropy of the sodium atom in low albite. American Mineralogist, 62, 921-933.

Always consult and cite the final, published document. See http://www.minsocam.org or GeoscienceWorld

Table 1. Experimental details of the applied instrumental techniques.

PXRD	
Instrument	Bruker-AXS D8
Operating power	40kV 40mA
Monochromator	Primary Ge(111)
Wavelength	CuKα1 (1.54056 Å)
Goniometer radius	21.75 cm
Detector, range	Linear PSD (Lynxeye), 3.3^{o}
Fixed divergence slit	0.2 mm (0.1^{o})
Receiving slit	8 mm
2theta range	10^{0} – 100°
Step size increment	0.02^{o}
Time per step	4 sec
Temperature	299(1) K
EMPA	
Instrument	JEOL JXA-8200
Operating power	15 kV 10 nA
Detectors (quantitative analysis)	WDS
Beam diameter	5 μm
Working distance	11 mm
Counting time	10 sec
EBSD	
Instrument	Phillips XL-30 FEG-ESEM
Operating power	20 keV (~0.8 nA)
Detector	Nordlys
Working distance	15 mm
Step size	0.3 μm (sample 16) 3 μm (sample 45)
SXRD	
Instrument	Bruker-AXS four-circle diffractometer
Operating power	40 kV 40 mA
Monochromator	flat graphite
Wavelength	MoKα (0.71073 Å)
Detector	area-detector Smart 1000CCD
Collimator	0.5 mm
Data collection range (2theta)	to 50°
Working distance	4 cm
Crystal rotation between exposures	0.2^{o}
Exposure	10 sec
Number of exposures per sample	2800
Temperature	299(1) K

Always consult and cite the final, published document. See http://www.minsocam.org or GeoscienceWorld

Table 2. Results of Rietveld refinement with (a) starting parameters from the literature (Armbruster et al. 1990; Blasi et al. 1987), (b) starting parameters from SXRD data.

	Sample 16		**Sample 45**	
	(a)	**(b)**	**(a)**	**(b)**
Rexp	3.27	3.27	3.32	3.33
Rwp	12.92	13.84	12.11	12.22
Rp	9.52	10.15	9.41	9.42
χ^2	3.95	4.24	3.64	3.67
Na-FELDSPAR				
RBragg	4.328	5.471	6.661	7.387
a (Å)	8.132(1)	8.131(1)	8.1430(3)	8.1424(3)
b (Å)	12.801(2)	12.796(2)	12.7897(4)	12.7893(4)
c (Å)	7.160(1)	7.158(1)	7.1612(2)	7.1609(2)
α (°)	94.099(6)	94.131(6)	94.260(2)	94.259(2)
β (°)	116.611(4)	116.609(4)	116.607(1)	116.607(1)
γ (°)	87.896(6)	87.871(6)	87.680(2)	87.681(2)
Crystallite size (nm)	180(7)	176(8)	1770(550)	1120(180)
Preferred orientation[a]	0.91(1); 0.503(7)	0.966(8); 0.415(7)	0.719(9); 0.573(5)	0.740(8); 0.555(5)
K-FELDSPAR				
Rbragg	5.073	5.825	6.546	6.492
a (Å)	8.582(1)	8.579(1)	8.5820(3)	8.5815(3)
b (Å)	12.967(2)	12.961(2)	12.9666(4)	12.9662(4)
c (Å)	7.194(1)	7.193(1)	7.2234(2)	7.2230(2)
α (°)	90.028(7)	90.046(7)	90.638(2)	90.636(2)
β (°)	116.103(4)	116.102(4)	115.958(2)	115.959(2)
γ (°)	89.627(6)	89.609(5)	87.700(2)	87.701(2)
Crystallite size (nm)	352(34)	327(32)	516(31)	439(22)
Preferred orientation[a]	0.942(8); 0.467(7)	0.930(8); 0.459(7)	0.782(8); 0.544(6)	0.803(7); 0.516(5)
Ab wt%	54	56	52	52
Or wt%	47	44	48	48

[a] for the (010) and the (001) planes, respectively.

Always consult and cite the final, published document. See http://www.minsocam.org or GeoscienceWorld

Table 3. Results of the chemical analysis (EMPA).

sample	oxide	K_2O	Na_2O	CaO	Fe_2O_3	Al_2O_3	SiO_2	Total
16 Na-feldspar[a]	wt%	0.13	11.91	0.29	0.08	19.38	67.87	99.66
	esd	0.17	0.16	0.02	0.05	0.26	0.88	1.15
	range	0.03-0.51	11.60-12.08	0.26-0.32	0.02-0.17	18.98-19.71	66.66-68.95	98.21-101.18
16 K-feldspar[b]	wt%	14.63	1.96	0.04	0.12	18.38	64.97	100.10
	esd	0.74	0.62	0.05	0.18	0.39	1.38	1.52
	range	13.65-15.91	0.89-2.67	0.00-0.13	0.01-0.56	17.85-18.86	63.16-67.52	98.37-103.40
45 Na-feldspar[c]	wt%	0.10	12.01	0.01	0.16	19.04	68.20	99.52
	esd	0.02	0.12	0.01	0.09	0.24	1.13	1.21
	range	0.07-0.14	11.77-12.15	0-0.03	0.02-0.26	18.64-19.50	66.57-69.98	98.05-101.18
45 K-feldspar[c]	wt%	16.92	0.43	0	0.06	18.11	65.03	100.56
	esd	0.23	0.08	-	0.05	0.20	0.79	1.03
	range	16.72-17.41	0.26-0.49	0	0-0.16	17.60-18.33	63.93-66.28	99.31-102.12

[a]Average of 7 points
[b]Average of 8 points
[c]Average of 10 points

Table 4. EBSD indexing parameters and summary of results

Sample No.; phase	Step I			Step III		
	Match unit	Indexing%	Twin laws	Match unit	Indexing%	Twin laws
16; K-feldspar	orthoclase (Prince et al. 1973)	18	Carlsbad (false)[a]	orthoclase (SXRD – this work)	21.2	None
16; Na-feldspar	low albite (Winter et al. 1977)	31.5	albite Carlsbad (false)[a]	low albite (SXRD – this work)	40.8	albite
45; K-feldspar	microcline (Finney 1962)	34.6	Carlsbad (false)[a]	microcline (SXRD – this work)	38.0	albite
45; Na-feldspar	bytownite (Fleet et al. 1966)	10.0	albite Carlsbad (false)[a]	low albite (SXRD – this work)	31.8	albite

[a]see text for explanation

Always consult and cite the final, published document. See http://www.minsocam.org or GeoscienceWorld

Table 5. Crystal lattice parameters and crystal structure refinement details.

	sample 16		sample 45	
ALBITE	C-setting	P-setting	C-setting	P-setting
a (Å)	8.133(2)	7.453	8.140(2)	7.445
b (Å)	12.81(1)	7.718	12.799(4)	7.721
c (Å)	7.171(2)	7.171	7.161(2)	7.161
α (°)	94.10(3)	107.17	94.22(2)	107.27
β (°)	116.59(3)	100.53	116.58(1)	100.45
γ (°)	87.79(1)	115.19	87.70(1)	115.11
V (Å^3)	666.9(8)	333.4	665.3(3)	332.7
Range of Miller indices[a]	-11<h<11 -18<k<18 -10<l<10		-9<h<9 -15<k<15 -8<l<8	
Non-overlapped reflections / unique	2754/1767		1705/1025	
K-FELDSPAR	C-setting	P-setting	C-setting	P-setting
a (Å)	8.598(2)	7.749	8.579(2)	7.636
b (Å)	12.970(3)	7.812	12.972(4)	7.913
c (Å)	7.200(1)	7.200	7.227(2)	7.227
α (°)	90.029(7)	104.05	90.57(2)	104.19
β (°)	116.137(5)	104.12	115.93(2)	103.72
γ (°)	89.498(8)	112.92	87.78(2)	113.06
V (Å^3)	720.8(3)	360.4	723(2)	361.5
Range of Miller indices[a]	-12<h<8 -18<k<18 -9<l<10		-10<h<10 -15<k<15 -8<l<8	
Non-overlapped reflections / unique	2382/1153		1906/1089	
global refinement details				
reflections total/I > 3σ	7035/6553		5265/3735	
parameters	238		239	
Goodness-of-fit, *S*[b]	3.26		2.25	
R / wR (I > 3σ)[c]	3.46% / 5.05%		4.47% / 5.78%	
R / wR (all data)[c]	3.69% / 5.09%		6.26% / 5.86%	
volume proportions a1:a2:k1:k2[d]	32:26:42		21:19:46:14	

[a] ranges are as for the C-setting
[b] $S = \{\Sigma[w(F_o^2-F_c^2)^2]/(n-p)\}^{1/2}$
[c] $R = \Sigma\,\big|\,|F_o|-|F_c|\,\big|/\Sigma|F_o|$; $wR = \{\Sigma[w(F_o^2-F_c^2)^2]/\Sigma[w(F_o^2)^2]\}^{1/2}$; $w = 1/\sigma^2$
F_o, F_c = observed and calculated structure factors, respectively
n, p = number of observations and number of parameters, respectively
[d] a1, a2 are albite twin components, k1, k2 K-feldspar twin components

Always consult and cite the final, published document. See http://www.minsocam.org or GeoscienceWorld

Table 6. Sizes of the coordination polyhedra of T (Si and Al) and A (Na) atomic sites in the crystal structures of Na-feldspars from samples 16, 45 and low albite (Armbruster et al. 1990).

Site	average bond length (Å)			volume of the coordination polyhedron (Å^3)		
	16	45	low albite	16	45	low albite
T_{1o} (Al)	1.739(7)	1.749(10)	1.742(5)	2.67(3)	2.72(4)	2.69(1)
T_{1m} (Si)	1.615(10)	1.615(16)	1.610(12)	2.16(3)	2.16(4)	2.14(1)
T_{2o} (Si)	1.616(12)	1.618(16)	1.615(15)	2.16(3)	2.17(4)	2.15(1)
T_{2m} (Si)	1.618(22)	1.623(24)	1.616(23)	2.17(3)	2.19(4)	2.16(1)
A[a] (Na)	2.79(38)	2.81(40)	2.79(40)	35.9(2)	36.3(3)	35.74(7)

[a]for the coordination number 9

Table 7. Sizes of the coordination polyhedra of T (Si and Al) and A (K and Na) atomic sites in the crystal structures of K-feldspars from samples 16, 45, A1D K-feldspar (Dal Negro et al. 1978), and maximum microcline (Blasi et al. 1987).

Site	average bond length (Å)				volume of the coordination polyhedron (Å^3)			
	16	A1D	45	microcline	16	A1D	45	microcline
T_{1o} (Al+Si))	1.680(5)	1.673(5)	1.740(5)	1.737(7)	2.42(1)	2.40(1)	2.69(2)	2.679(9)
T_{1m} (Si+Al)	1.654(9)	1.651(7)	1.622(20)	1.613(18)	2.31(1)	2.30(2)	2.18(2)	2.147(8)
T_{2o} (Si)	1.622(8)	1.623(9)	1.611(18)	1.614(18)	2.18(1)	2.19(1)	2.14(2)	2.152(8)
T_{2m} (Si)	1.622(9)	1.622(9)	1.616(24)	1.614(24)	2.18(1)	2.18(1)	2.16(2)	2.146(8)
A[a] (K+Na)	2.97(12)	2.97(13)	2.98(17)	2.97(17)	43.1(1)	43.1(1)	43.4(2)	43.2(2)

[a]for the coordination number 9

Always consult and cite the final, published document. See http://www.minsocam.org or GeoscienceWorld

Figure Captions

Figure 1. Flow chart illustrating the iterative, step-wise integration of the used analytical methods employed in this study (see text for details)

Figure 2. Backscatter Electron Image (BSE) of the (a) sample 16 and (b) sample 45 analyzed by EMPA; note the very fine laminations (1-10 μm width) of the two feldspar components (light versus dark grey) in sample 16, while for sample 45 domains of different feldspar are up to 100 μm wide

Figure 3. Sample 16. EBSD and EDS analysis: (a) band contrast image representing data quality (X mark surface features preventing EBSD analysis), (b) EDS map for Na α, (c) EDS map for K α, (d) phase distribution map after Step I (e) phase distribution map after Step III

Figure 4. Sample 45. EBSD and EDS analysis: (a) band contrast image representing data quality, (b) EDS map for Na α, (c) EDS map for K α, (d) phase distribution map after Step I (e) phase distribution map after Step III

Figure 5. Pole figures for sample 16 obtained by EBSD (upper and lower hemisphere projections). The two albite component orientations are shown as well as the K-feldspar orientation; note that the trace of the lamellar structure seen in Figure 5 is subparallel to the (010) plane.

Figure 6. Pole figures and crystallographic orientation map for sample 45; the trace of the boundary between K-feldspar and albite is parallel to the trace of the (100) plane.

Figure 7. Photograph of the thin section from sample 45. Crossed polars. Field of view (horizontal) is 600 μm.

Figure 8. Relations of the volumes of coordination polyhedra for the tetrahedral sites in the two K-feldspars. The horizontal axis represents all sites, the vertical only the largest one.

Always consult and cite the final, published document. See http://www.minsocam.org or GeoscienceWorld

Open circles are for sample 16, filled squares for sample 45. The lines represent the expected trends for the two step (full) or one step (stippled) ordering process.

Figure 9. Textural component maps for sample 45 for all feldspar components, showing a spread of orientation of up to 6º across the whole analysed area

Always consult and cite the final, published document. See http://www.minsocam.org or GeoscienceWorld

Deposited material, online resource captions

OR 1. Crystal structure information and list of observed and calculated structure factors for the albite component in sample 16

OR 2. Crystal structure information and list of observed and calculated structure factors for the K-feldspar component in sample 16

OR 3. Crystal structure information and list of observed and calculated structure factors for the albite component in sample 45

OR 4. Crystal structure information and list of observed and calculated structure factors for the K-feldspar component in sample 45

OR 5. Orientation and relation matrices for crystallographic components and the list of reflections in HKL5 format for the sample 16

OR 6. Orientation and relation matrices for crystallographic components and the list of reflections in HKL5 format for the sample 45

Always consult and cite the final, published document. See http://www.minsocam.org or GeoscienceWorld

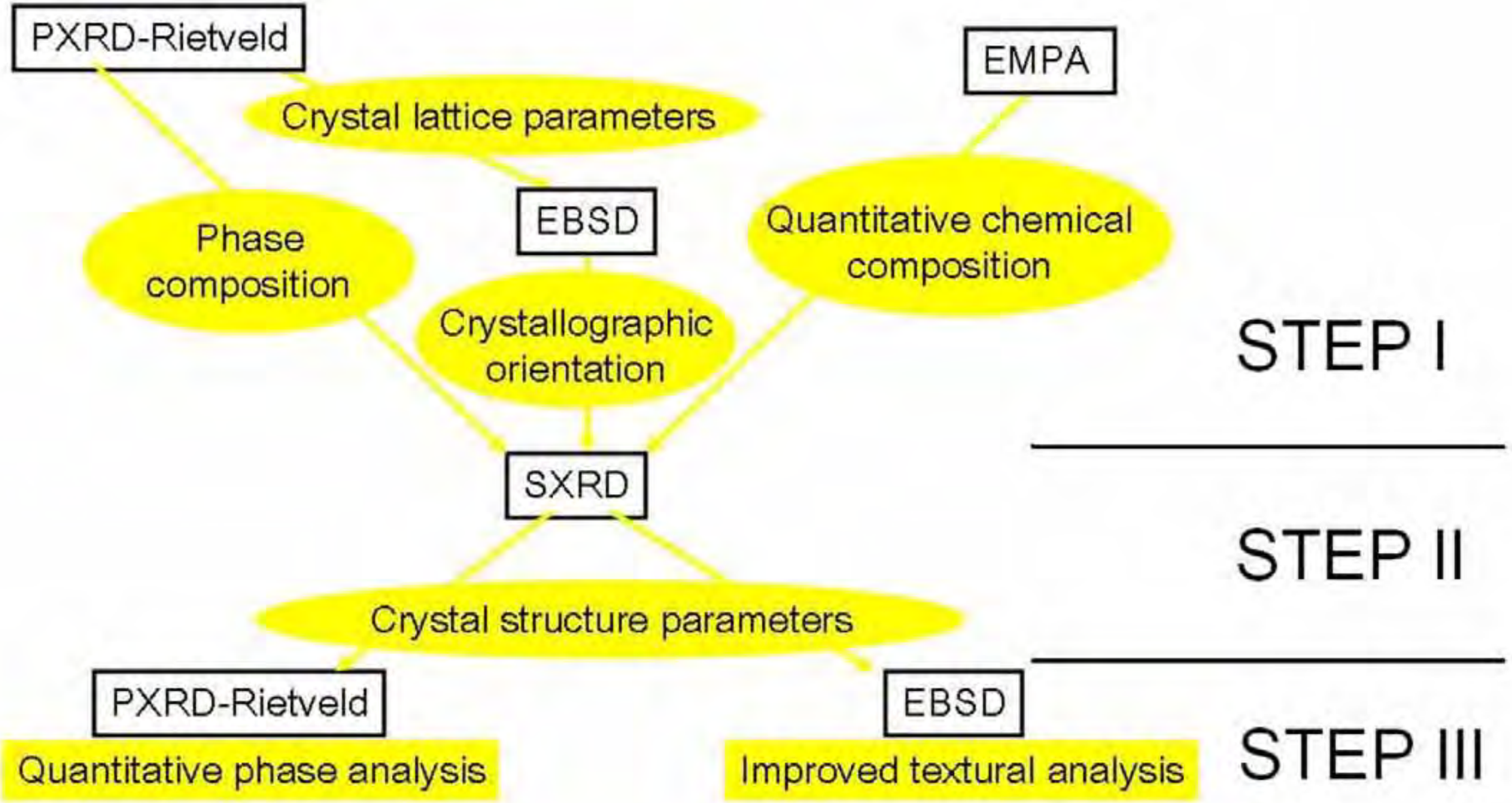
PXRD-Rietveld
Crystal lattice parameters
EMPA
Phase composition
EBSD
Quantitative chemical composition
Crystallographic orientation
STEP I
SXRD
STEP II
Crystal structure parameters
PXRD-Rietveld
EBSD
Quantitative phase analysis
Improved textural analysis
STEP III

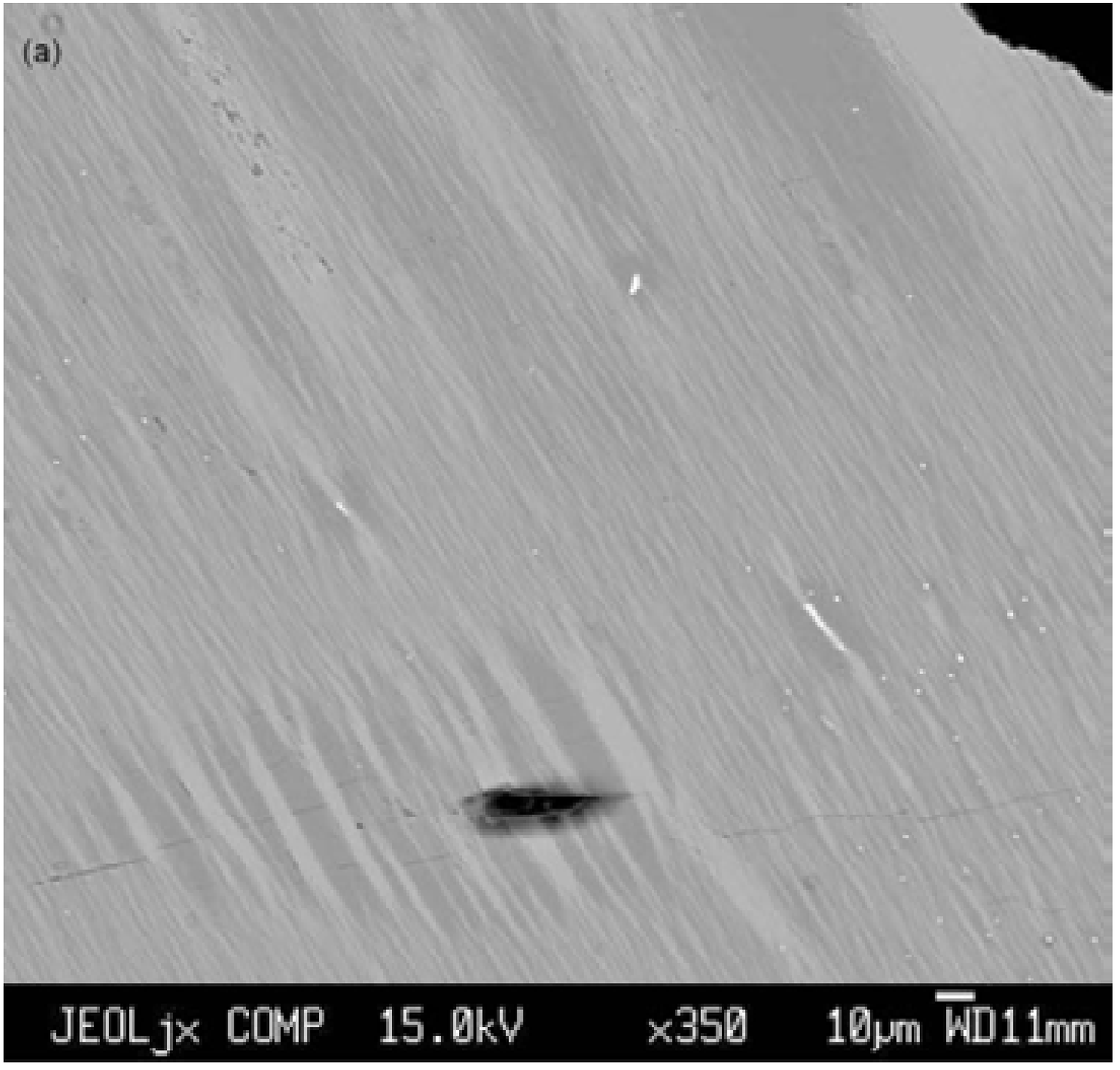
(a)
JEOLjx COMP 15.0kV x350 10μm WD11mm

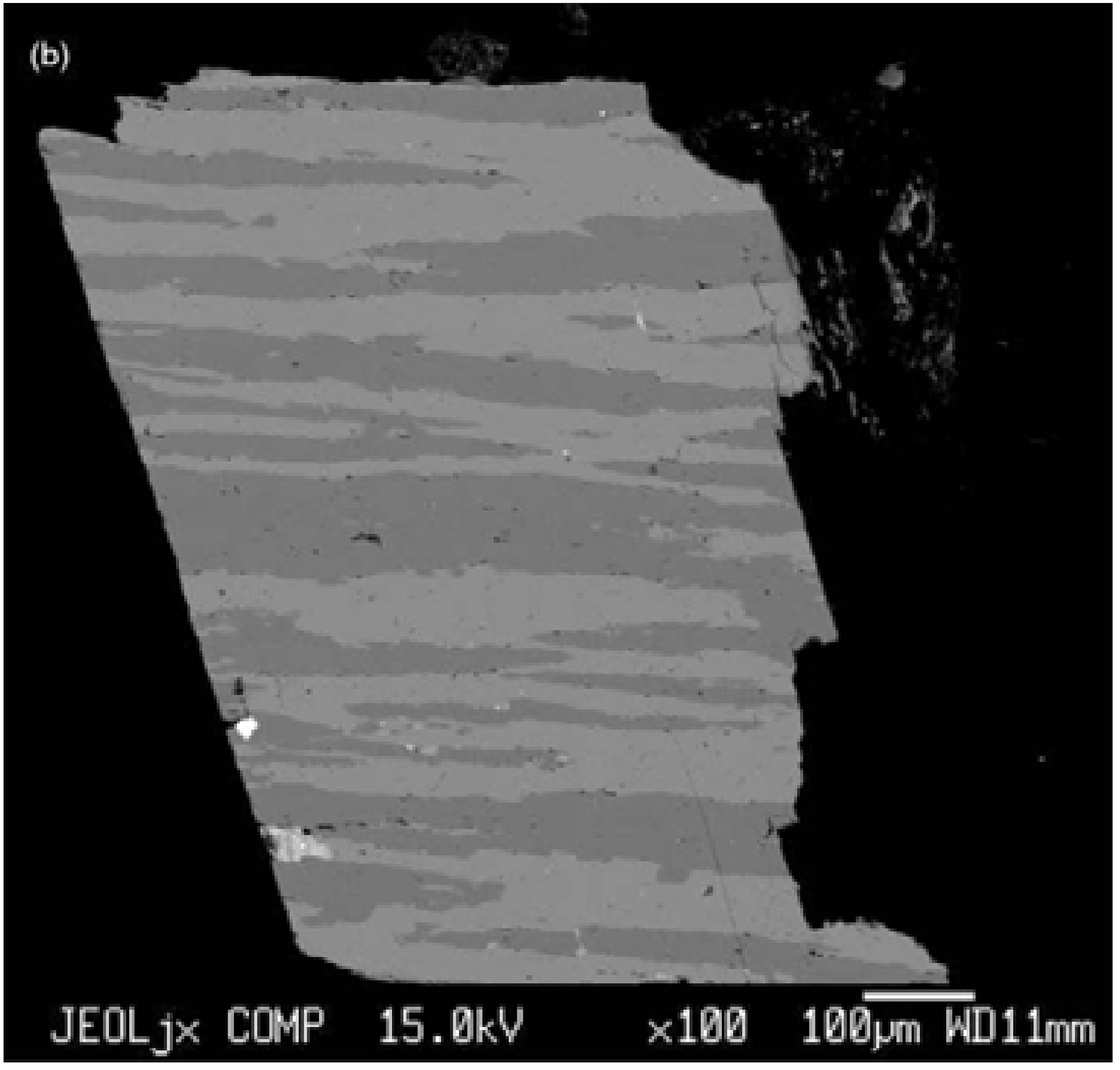
(b)
JEOLjx COMP 15.0kV ×100 100μm WD11mm

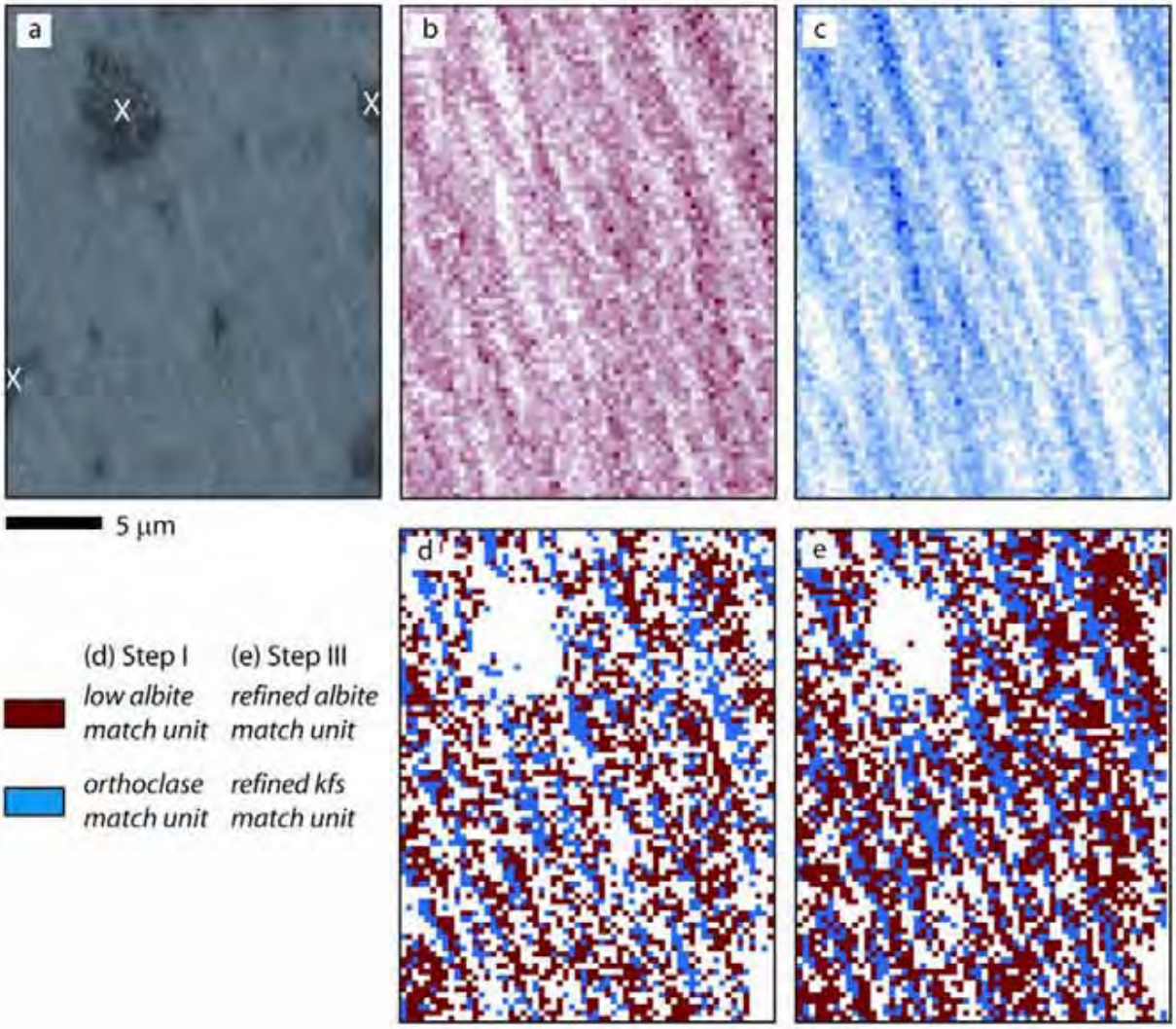
a
X
X
X
b
c
5 µm
d
e
(d) Step I
(e) Step III
low albite match unit
refined albite match unit
orthoclase match unit
refined kfs match unit

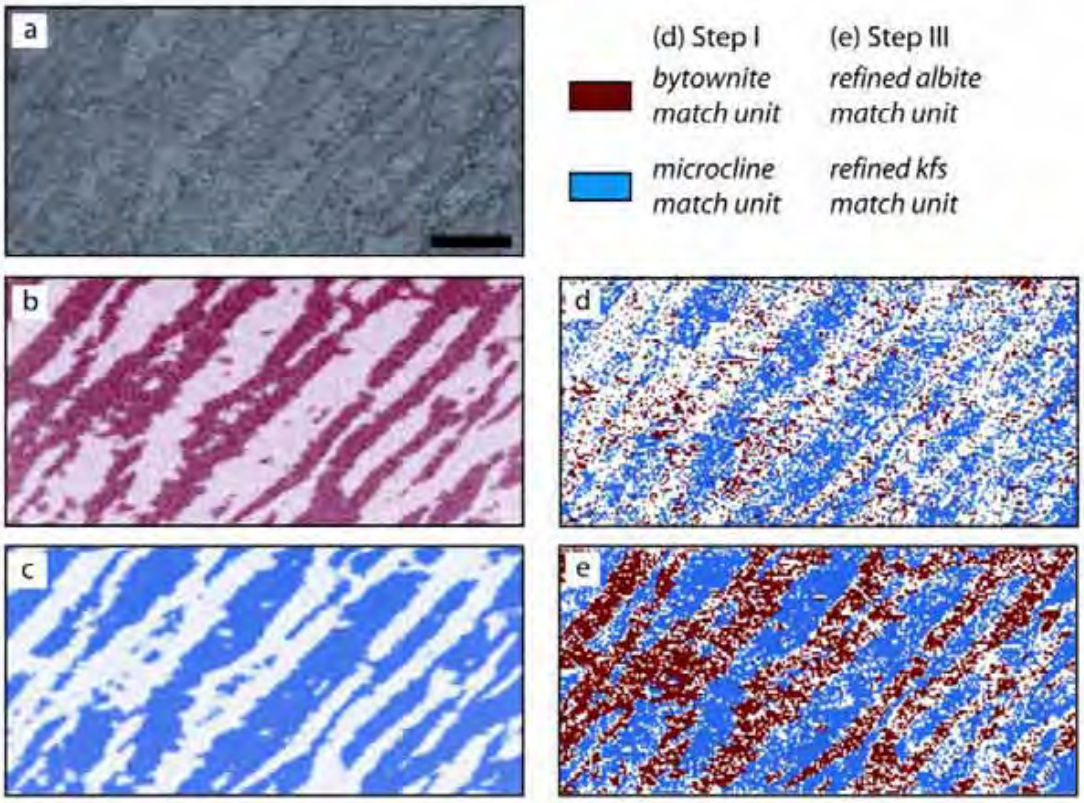

scale bar = 100 μm

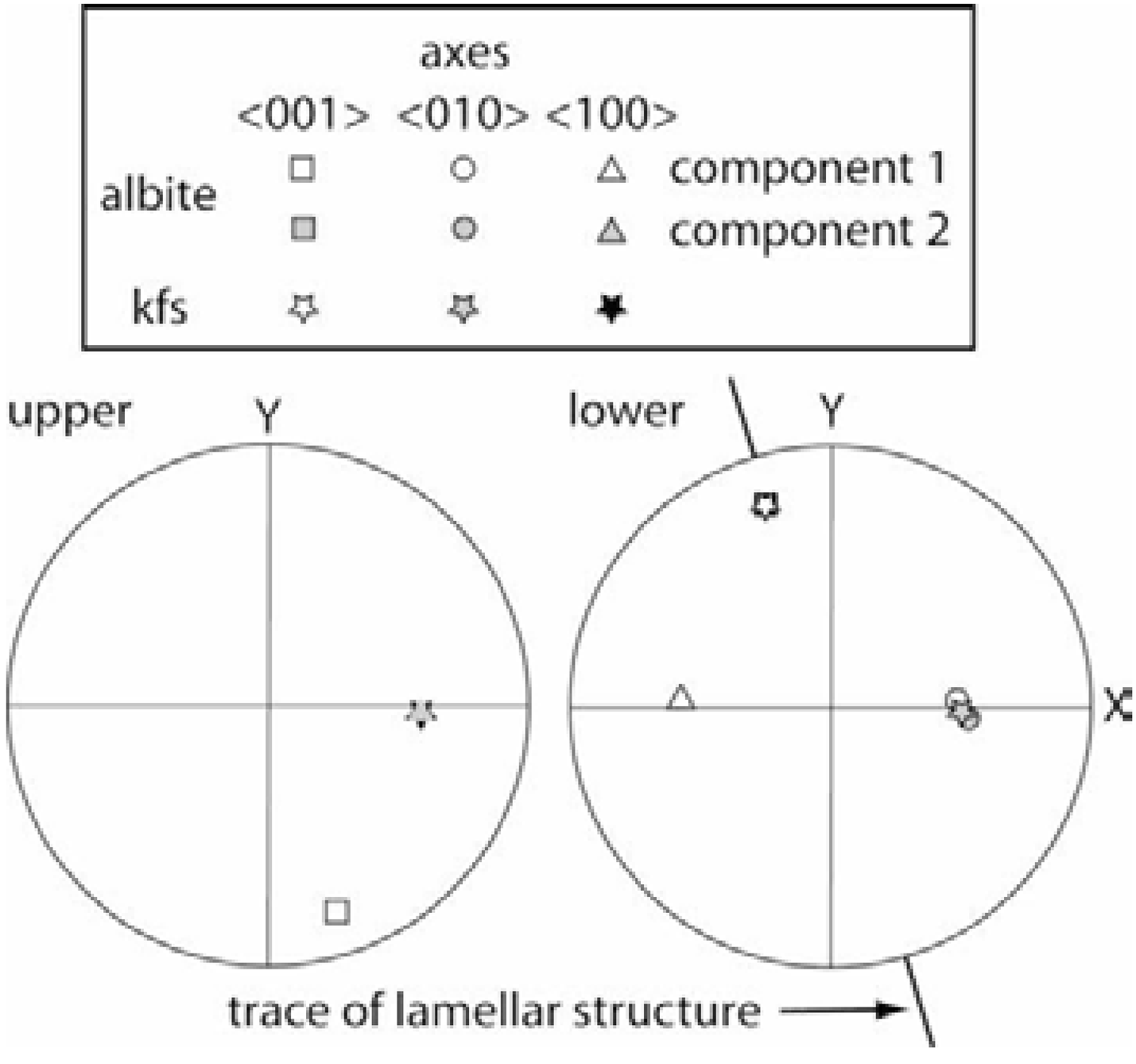
axes
<001> <010> <100>
albite
component 1
component 2
kfs
upper
Y
lower
Y
X
trace of lamellar structure

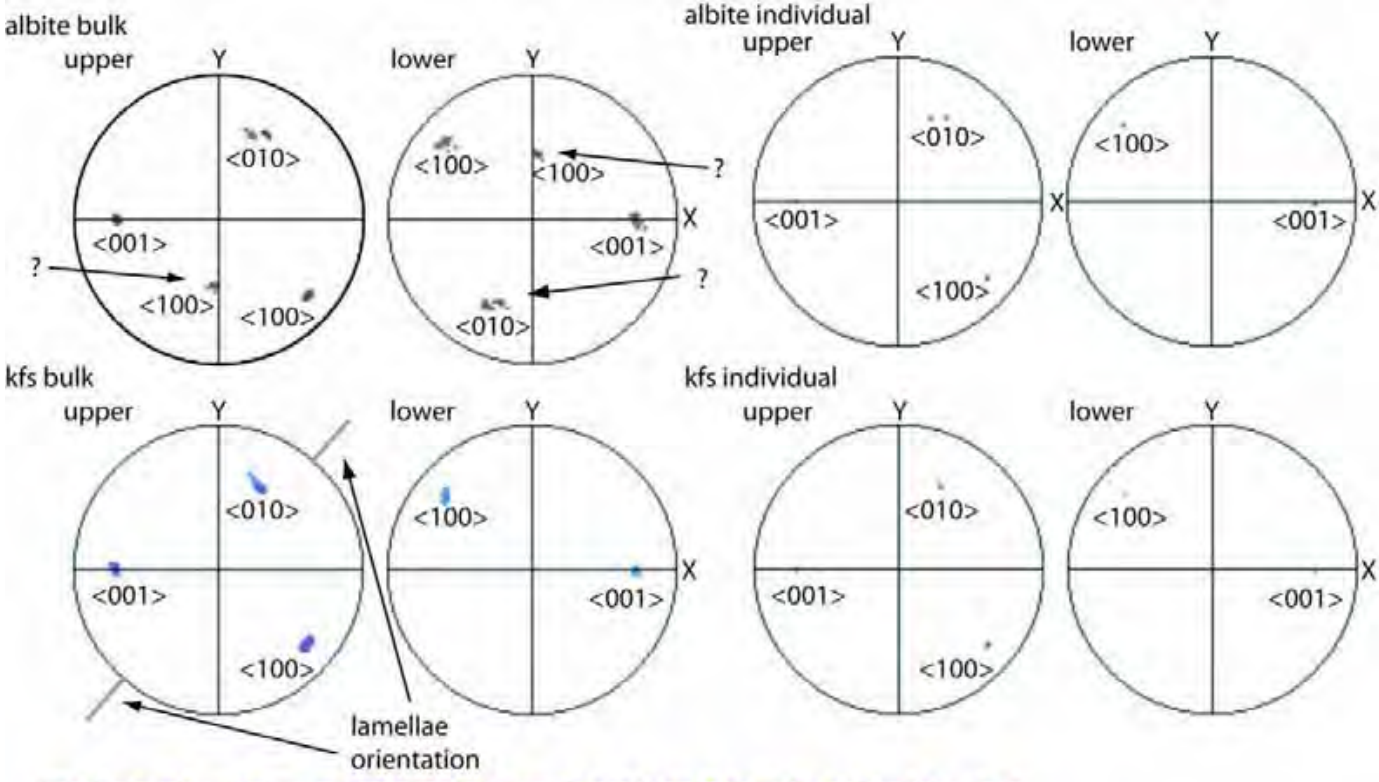
albite bulk
upper
lower
albite individual
upper
lower
kfs bulk
upper
lower
kfs individual
upper
lower
Y
X
<010>
<100>
<001>
?
lamellae
orientation

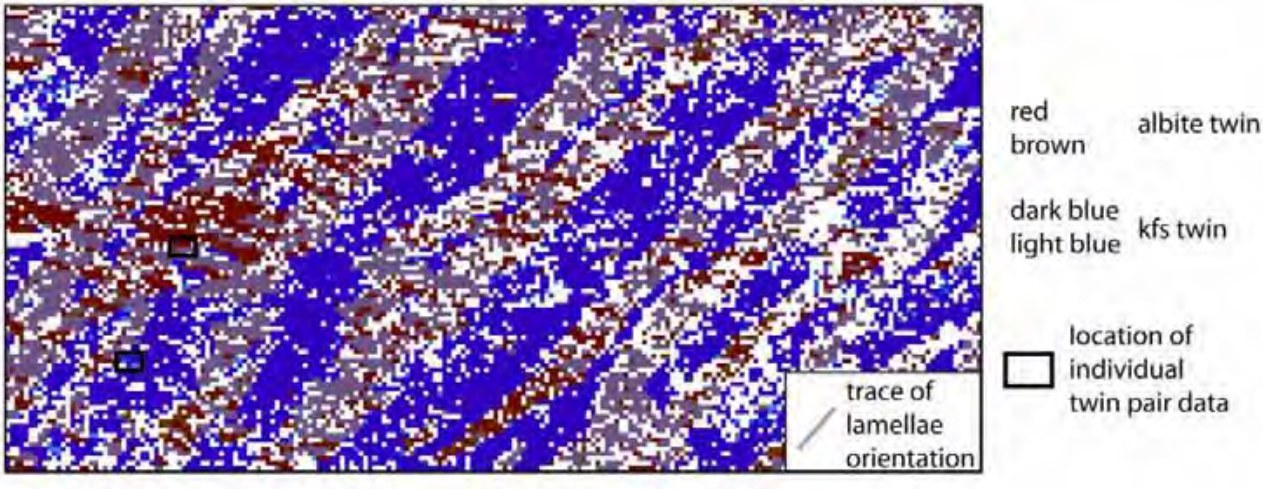
red
brown
albite twin
dark blue
light blue
kfs twin
location of
individual
twin pair data
trace of
lamellae
orientation

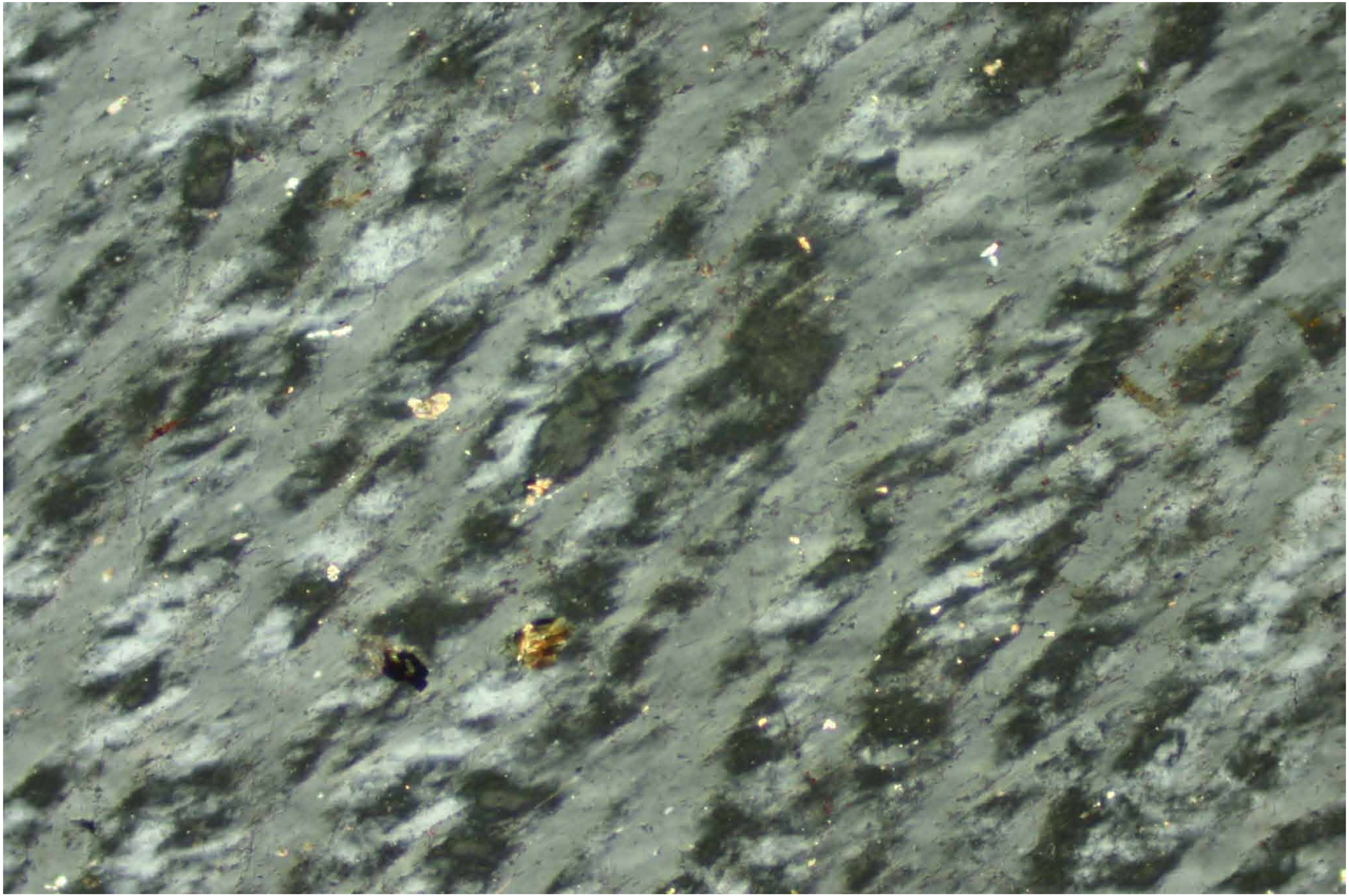

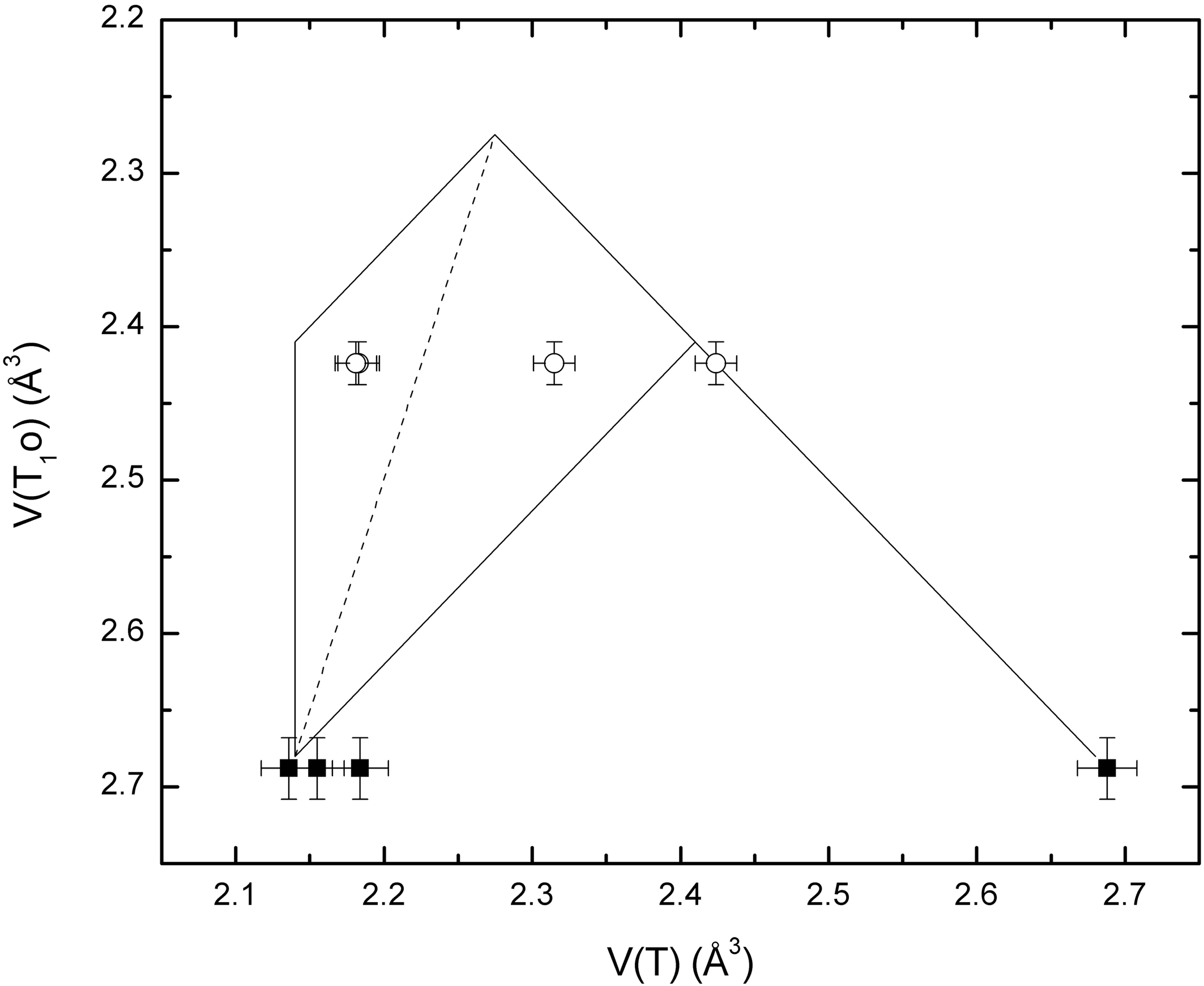
2.2
2.3
2.4
2.5
2.6
2.7
V(T1O) (Å3)
2.1
2.2
2.3
2.4
2.5
2.6
2.7
V(T) (Å3)

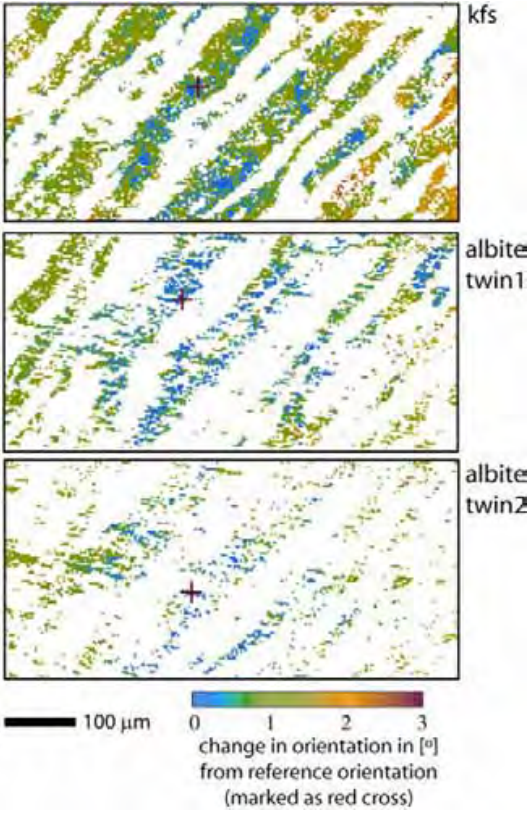
kfs
albite
twin1
albite
twin2
100 µm
0
1
2
3
change in orientation in [°]
from reference orientation
(marked as red cross)